

Harnessing the Potential of Omnidirectional UAVs in RIS-Enabled Wireless Networks

Abdoul Karim A. H. Saliah¹, Hajar El Hammouti¹, Daniel Bonilla Licea^{1,2}

¹College of Computing, Mohammed VI Polytechnic University (UM6P), Benguerir, Morocco.

²Faculty of Electrical Engineering, Czech Technical University in Prague, Czech Republic.

Email: {abdoul.saliah, hajar.elhammouti, daniel.bonilla}@um6p.ma

Abstract—Multirotor Aerial Vehicles (MRAVs) when integrated into wireless communication systems and equipped with a Reflective Intelligent Surface (RIS) enhance coverage and enable connectivity in obstructed areas. However, due to limited degrees of freedom (DoF), traditional under-actuated MRAVs with RIS are unable to control independently both the RIS orientation and their location, which significantly limits network performance. A new design, omnidirectional MRAV (o-MRAV), is introduced to address this issue. In this paper, an o-MRAV is deployed to assist a terrestrial base station in providing connectivity to obstructed users. Our objective is to maximize the minimum data rate among users by optimizing the o-MRAV’s orientation, location, and RIS phase shift. To solve this challenging problem, we first smooth the objective function and then apply the Parallel Successive Convex Approximation (PSCA) technique to find efficient solutions. Our simulation results show significant improvements of 28% and 14% in terms of minimum and average data rates, respectively, for the o-MRAVs compared to traditional u-MRAVs.

Index Terms—Communication-aware robotics, UAVs, omnidirectional MRAV (o-MRAV), reflective Intelligent Surface (RIS), relays, UAVs.

I. INTRODUCTION

In the past decade, the incorporation of unmanned aerial vehicles (UAVs) into wireless networks has attracted substantial interest from both academia and industry [1]. UAVs have been explored for a variety of applications, including improving network coverage, disaster recovery, and data collection [2]–[5]. Within this context, a substantial portion of research has focused on multirotor aerial vehicles (MRAVs), with particular emphasis on a design known as under-actuated MRAVs (u-MRAVs) [6]. These UAVs are characterized by having fewer actuation inputs—such as thrust, pitch, roll, and yaw angles—than degrees of freedom (DoF), which include their 3D position and orientation. As a result, the 3D orientation of u-MRAVs depends on their translational velocity, making it impossible to achieve independent control of both 3D position and 3D orientation [6], [7].

Recently, the robotics community has introduced new MRAV designs, referred to as omnidirectional MRAVs (o-

MRAVs). These designs allow the total thrust vector to be controlled in all directions, independently of torque, with multiple input combinations. This results in more actuation inputs than degrees of freedom, which enables complete and independent control over each movement axis, and allows precise orientation management [6], [8], [9].

To further enhance the versatility of UAVs in wireless networks, another promising technology has been considered: reconfigurable intelligent surfaces (RIS). RIS can be deployed to efficiently redirect signals toward users in obstructed areas and improve overall communication performance. This has given rise to the concept of aerial RIS (ARIS), which aims to dynamically position RIS in 3D space using a UAV.

Several works have investigated the 3D position of an ARIS for multiple purposes. For instance, RIS placement and 3D passive beamforming are optimized in [10] to enhance the worst signal-to-noise ratio. In [11], a high aerial platform (HAP) enabled by RIS is examined for redirecting backhaul signals to UAVs. The authors propose a joint optimization of positioning and RIS phase shifts to improve system energy efficiency. Additionally, the case of multiple ARIS is explored in [12], where deep reinforcement learning is applied to jointly optimize ARIS placement, phase shifts, and power control. However, only a limited number of research papers have explored the impact of RIS orientation. In [13], the rotation of the RIS plane is examined to enhance network capacity. Similarly, in [14], the authors investigate the optimal orientation of a RIS to improve the data rate for a single user. Additionally, [15] focuses on adjusting RIS orientation to improve localization accuracy in indoor environments.

This paper, motivated by the previous studies on the effect of the orientation of the RIS, explores the deployment of o-MRAVs equipped with RIS and shows the benefits that the optimization of the RIS orientation and position brings to the network performance. In particular, we analyze how control over the orientation of the RIS, in addition to phase shift and 3D position, can significantly enhance the minimum data rate for users in obstructed environments. To the best of our knowledge, this is the first work to explore the integration of RIS with o-MRAVs and to offer new insights into their potential to enhance wireless networks.

Notations: y is a scalar, \mathbf{y} or \mathbf{Y} is a vector or matrix. \mathbf{Y}^T and \mathbf{Y}^* denote the transpose, and Hermitian of \mathbf{Y} , respectively. $|\cdot|$ denotes the modulus of a complex number and

This document has been produced with the financial assistance of the European Union (Grant no. DCI-PANAF/2020/420-028), through the African Research Initiative for Scientific Excellence (ARISE), pilot programme. ARISE is implemented by the African Academy of Sciences with support from the European Commission and the African Union Commission. The contents of this document are the sole responsibility of the author(s) and can under no circumstances be regarded as reflecting the position of the European Union, the African Academy of Sciences, and the African Union Commission.

$\|\cdot\|_2$ denotes the l_2 -norm. j is the imaginary unit. $\text{mod}(\cdot, \cdot)$ is the modulus and $\lfloor \cdot \rfloor$ is the floor function.

II. SYSTEM MODEL

We consider a communication model where a base station B communicates with K user equipments (UEs) in an obstructed environment. As a result, there exists no direct link between the base station and the UEs, as illustrated in Fig.1. To overcome this problem, an o-MRAV equipped with a RIS ensures the scattering of the signal received from the base station towards the UEs. We also assume that the base station is equipped with a linear antenna array separated by a vertical distance d_{V_0} , and the set of antenna elements is denoted by $\mathcal{N} = \{1, \dots, N\}$. To reflect the signal, the o-MRAV carries an RIS consisting of $M = M_H \times M_V$ elements, arranged in a uniform rectangular array. The horizontal and vertical separation distances between RIS elements are denoted by d_{H_R} and d_{V_R} , respectively. The set of RIS elements is given by $\mathcal{M} = \{1, \dots, M\}$ and the set of UEs is denoted by $\mathcal{K} = \{1, \dots, K\}$. For the sake of notation, in the remainder of the paper, we designated k to represent a user, R to represent the RIS, and B to represent the base station.

We consider two reference coordinate systems: the global reference system (O_G, X, Y, Z) , centered at the base station antenna, and the mobile body reference system (O_R, x_b, y_b, z_b) , centered at the MRV center. In the global reference system, the positions of the base station antenna, the MRV, and any user equipment (UE) $k \in \mathcal{K}$ are denoted by $\mathbf{p}_B = [x_B, y_B, z_B]^T$, $\mathbf{p}_R = [x_R, y_R, z_R]^T$, and $\mathbf{p}_k = [x_k, y_k, z_k]^T$, respectively. Additionally, the position of an individual antenna element $n \in \mathcal{N}$ in the global reference system is expressed as

$$\mathbf{p}_n^B = [d_{H_0}, 0, (n-1)d_{V_0}]^T, \forall n \in \mathcal{N}, \quad (1)$$

where d_{H_0} represents the horizontal width of the BS antenna array. Similarly, the position of a RIS element $m \in \mathcal{M}$ in the mobile body reference system is given by [16]

$$\mathbf{p}_m^R = [\lfloor (m-1)/M_V \rfloor d_{V_R}, \text{mod}((m-1), M_H) d_{H_R}, 0]^T. \quad (2)$$

The o-MRAV is capable of changing its orientation independently of its position. To describe its orientation, we use Euler angles with XYZ convention: roll (φ), pitch (ϑ), and yaw (ψ). Consequently, the orientation of the o-MRAV is represented as a vector $\boldsymbol{\Omega} = [\varphi, \vartheta, \psi]^T \in \mathbb{R}^3$.

The orientation $\boldsymbol{\Omega}$ directly impacts the positions of RIS elements in the global reference system. Specifically, the vector $\mathbf{p}_{1-m}^R(\boldsymbol{\Omega})$, which represents the position of any RIS element m relative to the first RIS element in the global reference system is given by

$$\mathbf{p}_{1-m}^R(\boldsymbol{\Omega}) = \mathcal{R}_\Omega(\mathbf{p}_m^R - \mathbf{p}_1^R), \forall m \in \mathcal{M}, \quad (3)$$

with \mathcal{R}_Ω the rotation matrix from the body reference to the global reference, which is given by

$$\mathcal{R}_\Omega = \begin{bmatrix} c_\vartheta c_\psi & -c_\vartheta s_\psi & s_\vartheta \\ c_\varphi s_\psi + c_\psi s_\varphi s_\vartheta & c_\varphi c_\psi - s_\varphi s_\vartheta s_\psi & -c_\vartheta s_\varphi \\ s_\varphi s_\psi - c_\varphi c_\psi s_\vartheta & c_\psi s_\varphi + c_\varphi s_\vartheta s_\psi & c_\varphi c_\vartheta \end{bmatrix}, \quad (4)$$

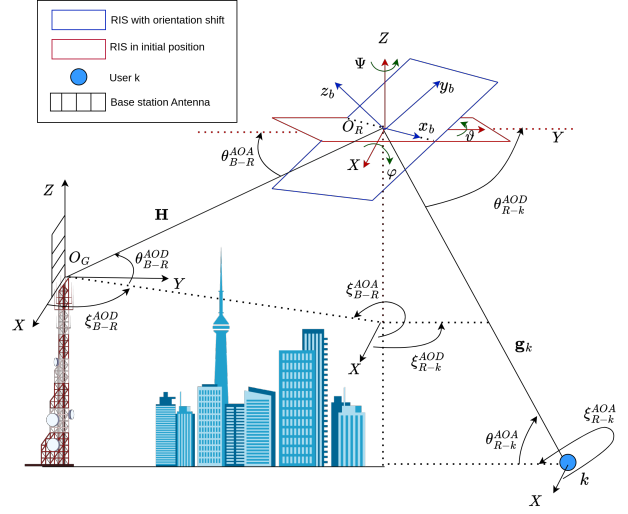


Fig. 1. Communication Model

where s_\cdot and c_\cdot are respectively sine and cosine functions.

We define the channel between the base station and the o-MRAV as $\mathbf{H} \in \mathbb{C}^{N \times M}$, and the channel between the o-MRAV and any given user k as $\mathbf{g}_k \in \mathbb{C}^{M \times 1}$. They are expressed as

$$\mathbf{H} = \eta_{B-R} \mathbf{a}_{rx,R}(\theta_{B-R}^{AOA}, \xi_{B-R}^{AOA}, \boldsymbol{\Omega}) \mathbf{a}_{tx,B}^*(\theta_{B-R}^{AOD}, \xi_{B-R}^{AOD}), \quad (5)$$

$$\mathbf{g}_k = \eta_{R-k} \mathbf{a}_{tx,R}^*(\theta_{R-k}^{AOD}, \xi_{R-k}^{AOD}, \boldsymbol{\Omega}), \quad (6)$$

with $\eta_{B-R} = \frac{\sqrt{\beta_0}}{d_{B-R}} e^{-j2\pi d_{B-R}/\lambda}$ and $\eta_{R-k} = \frac{\sqrt{\beta_0}}{d_{R-k}} e^{-j2\pi d_{R-k}/\lambda}$, where β_0 is the reference path gain at a distance of 1 meter. The distances $d_{B-R} = \|\mathbf{p}_R - \mathbf{p}_k\|_2$ and $d_{R-k} = \|\mathbf{p}_k - \mathbf{p}_R\|_2$ represent the distances between the base station and the RIS, and between the RIS and user k , respectively. The angles $(\theta_{B-R}^{AOD}, \xi_{B-R}^{AOD})$ and $(\theta_{B-R}^{AOA}, \xi_{B-R}^{AOA})$ denote the angles of departure and arrival for the channel between the base station and the RIS. Similarly, $(\theta_{R-k}^{AOD}, \xi_{R-k}^{AOD})$ represent the angles of departure for the channel between the RIS and user k . $\mathbf{a}_{tx,B}$, $\mathbf{a}_{rx,R}$ and $\mathbf{a}_{tx,R}$ denotes respectively the transmit array response of the base station, RIS receive array response and RIS transmit array response. They are given by

$$\mathbf{a}_{tx,B}(\theta_{B-R}^{AOD}, \xi_{B-R}^{AOD}) = \begin{bmatrix} e^{js(\theta_{B-R}^{AOD}, \xi_{B-R}^{AOD}) \mathbf{p}_1^B} \\ \dots, e^{js(\theta_{B-R}^{AOD}, \xi_{B-R}^{AOD}) \mathbf{p}_N^B} \end{bmatrix}^T, \quad (7)$$

$$\mathbf{a}_{rx,R}(\theta_{B-R}^{AOA}, \xi_{B-R}^{AOA}, \boldsymbol{\Omega}) = \begin{bmatrix} e^{js(\theta_{B-R}^{AOA}, \xi_{B-R}^{AOA}) \mathbf{p}_{1-1}^R(\boldsymbol{\Omega})} \\ \dots, e^{js(\theta_{B-R}^{AOA}, \xi_{B-R}^{AOA}) \mathbf{p}_{1-M}^R(\boldsymbol{\Omega})} \end{bmatrix}^T, \quad (8)$$

$$\mathbf{a}_{tx,R}(\theta_{R-k}^{AOD}, \xi_{R-k}^{AOD}, \boldsymbol{\Omega}) = \begin{bmatrix} e^{js(\theta_{R-k}^{AOD}, \xi_{R-k}^{AOD}) \mathbf{p}_{1-1}^R(\boldsymbol{\Omega})} \\ \dots, e^{js(\theta_{R-k}^{AOD}, \xi_{R-k}^{AOD}) \mathbf{p}_{1-M}^R(\boldsymbol{\Omega})} \end{bmatrix}^T, \quad (9)$$

where $\mathbf{s}(\theta_{W-Z}, \xi_{W-Z})$ represents a wave vector, which indicates the phase variation of a plane wave at a given position in

the global reference. Its expression is given by [17] as follows

$$\mathbf{s}(\theta_{w-z}, \xi_{w-z}) = \frac{2\pi}{\lambda} \begin{bmatrix} \cos(\theta_{w-z}) \cos(\xi_{w-z}), \\ \cos(\theta_{w-z}) \sin(\xi_{w-z}), \sin(\theta_{w-z}) \end{bmatrix}, \quad (10)$$

where θ_{w-z} and ξ_{w-z} denote the elevation angle and the azimuth angle, respectively, of the channel between the transmitter W and the receiver Z .

Accordingly, the data rate of a given user k is defined by

$$R_k = B_k \log_2 \left(1 + \frac{P_0 G_A |\mathbf{g}_k \mathbf{M}_\Theta \mathbf{H} \mathbf{f}|^2}{\sigma_0^2} \right), \forall k \in \mathcal{K}, \quad (11)$$

where B_k is the bandwidth allocated to user k , P_0 is the power of transmission of the base station, G_A the gain of the base station antenna, the reflection matrix of the RIS is $\mathbf{M}_\Theta = \text{diag}(\{e^{j\theta_i}\}_{i=1}^M)$ with $\Theta = (\theta_1, \dots, \theta_M)$, \mathbf{f} is the beamforming vector at the base station and σ_0^2 is the variance of an additive white Gaussian noise. We consider that a maximum ratio strategy (MRT) is applied to maximize the signal-to-noise ratio at the base station [18] [11]. This results in beamforming that depends only on the array response at the base station through the following expression [11]

$$\mathbf{f} = \mathbf{a}_{t,x,B}(\theta_{B-R}^{AOD}, \xi_{B-R}^{AOD}) / \|\mathbf{a}_{t,x,B}(\theta_{B-R}^{AOD}, \xi_{B-R}^{AOD})\|_2. \quad (12)$$

Furthermore, we assume, for the sake of tractability, that the channels \mathbf{H} and \mathbf{g}_k are known at the base station. This can be achieved through the use of channel estimation techniques [19]. Additionally, we consider the use of frequency division multiple access (FDMA) at the base station to ensure that there is no interference.

III. MINIMUM RATE OPTIMIZATION

This work aims to maximize the minimum rate among users by optimizing the o-MRAV orientation and position in addition to the RIS reflection matrix. The purpose of this work is to demonstrate that incorporating o-MRAV orientation alongside position and phase shift optimization yields significant gains compared to traditional approaches with fixed orientation. The optimization problem is expressed as follows

$$\max_{\Omega, \mathbf{p}_R, \Theta} \left(\min_{k \in \mathcal{K}} R_k \right) \quad (13)$$

$$\text{s.t.} \quad \varphi \in \left[0, \frac{\pi}{2}\right], \vartheta \in \left[0, \frac{\pi}{2}\right], \psi \in [0, 2\pi), \quad (13a)$$

$$\theta_m \in [0, 2\pi], \forall m \in \mathcal{M}, \quad (13b)$$

$$\mathbf{p}_R^T \in [x_{\min}, x_{\max}] \times [y_{\min}, y_{\max}] \times [z_{\min}, z_{\max}]. \quad (13c)$$

In this problem, constraint (13a) limits the UAV orientation to keep the RIS visible to the base station and users, (13b) defines the range of the phase shift of RIS elements and constraint (13c) delimits the region covered by the UAV.

This problem is a challenging one as it is a non-convex one. Moreover, the minimum term in the maximization problem further complicates the problem because of the non-smooth nature of the min function.

Algorithm 1 Parallel Successive Convex Approximation (PSCA)

- 1: Set $l = 0$, initialize with a feasible point $\mathbf{x}^0 \in \mathcal{X}$, and $\{\gamma^l\} \in (0, 1]$.
 - 2: **repeat**
 - 3: **for all** $i \in \{1, 2, 3\}$ **(in parallel) do**
 - 4: Solve (16)
 - 5: **end for**
 - 6: Compute the next iterate:
 - 7: $\mathbf{x}^{l+1} = \mathbf{x}^l + \gamma^l (\hat{\mathbf{x}}(\mathbf{x}^l) - \mathbf{x}^l)$
 - 8: $l \leftarrow l + 1$
 - 9: **until** convergence
 - 10: **return** \mathbf{x}^l
-

To overcome this problem, we first approximate the min function using the p -norm, which provides a close approximation when $p \rightarrow -\infty$ [20]. The studied problem is then reformulated as

$$\max_{\Omega, \mathbf{p}_R, \Theta} \|(R_1, \dots, R_K)\|_p \quad (14)$$

$$\text{s.t.} \quad (13a), (13b), (13c) \quad (14a)$$

We consider the convex feasible set of solutions of the problem to be $\mathcal{X} = \mathcal{X}_1 \times \mathcal{X}_2 \times \mathcal{X}_3$, where $\mathcal{X}_1 = [0, 2\pi]^M$, $\mathcal{X}_2 = [x_{\min}, x_{\max}] \times [y_{\min}, y_{\max}] \times [z_{\min}, z_{\max}]$, and $\mathcal{X}_3 = [0, \frac{\pi}{2}]^2 \times [0, 2\pi]$ are respectively the RIS phase shift, the MRAV position and orientation. We then obtain the following problem

$$\min_{\mathbf{x}_1, \mathbf{x}_2, \mathbf{x}_3} F(\mathbf{x}_1, \mathbf{x}_2, \mathbf{x}_3) = -\|(R_1, \dots, R_K)\|_p \quad (15)$$

$$\text{s.t.} \quad \mathbf{x}_i \in \mathcal{X}_i, \forall i \in \{1, 2, 3\}, \quad (15a)$$

This results in a non-convex multi-block optimization problem, which we address using the Parallel Successive Convex Approximation (PSCA) method.

The PSCA as described in Algorithm 1 consists of iteratively solving convex approximations of the objective function for all blocks. First, at each iteration l , the following convex problems are solved in parallel

$$\hat{\mathbf{x}}_i(\mathbf{x}^l) = \arg \min_{\mathbf{x}_i \in \mathcal{X}_i} \tilde{F}_i(\mathbf{x}_i | \mathbf{x}^l), \forall i \in \{1, 2, 3\} \quad (16)$$

where $\tilde{F}_i(\mathbf{x}_i | \mathbf{x}^l)$ is the first-order Taylor expansion of F around \mathbf{x}^l with respect to \mathbf{x}_i . Second, the next iterate \mathbf{x}^{l+1} is computed in step 7 by linear combination of the obtained optimal $\hat{\mathbf{x}}_i(\mathbf{x}^l)$ and \mathbf{x}^l . This process is repeated until convergence. The complexity analysis of the PSCA method is thoroughly discussed in [21].

IV. SIMULATION RESULTS

To assess the performance of an o-MRAV mounted with RIS, we consider an area of $1000\text{m} \times 1000\text{m}$ where $K = 10$ users are randomly distributed on the ground. A base station at an altitude $h_{BS} = 68\text{m}$ is positioned at the center of the global reference and has $N = 10$ antenna elements. The signal emitted by the base station has a wavelength of $\lambda = 0.15\text{m}$. The base station transmits with a power of $P_0 = 1\text{W}$ and an antenna gain of $G_A = 8\text{dB}$. The horizontal and vertical distances between the base station's antenna elements are

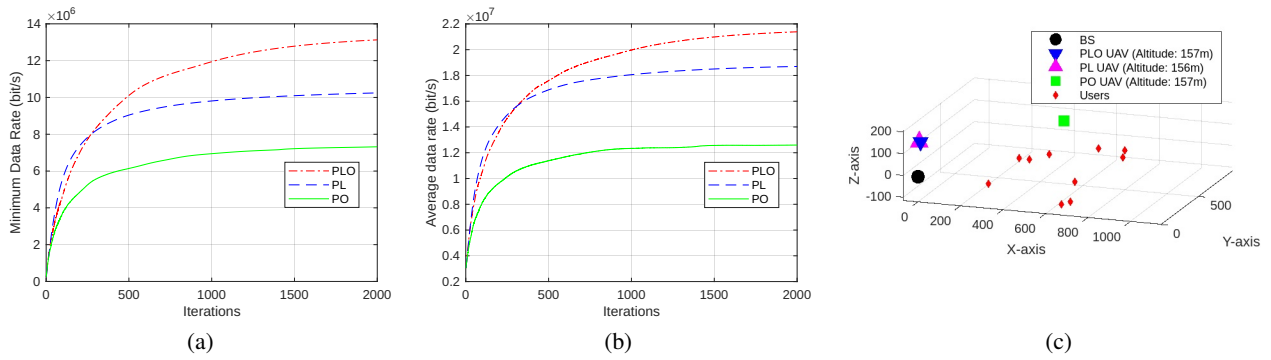


Fig. 2. (a) Minimum rate vs iterations, (b) Average rate vs iterations, (c) Optimized positions of o-MRAV.

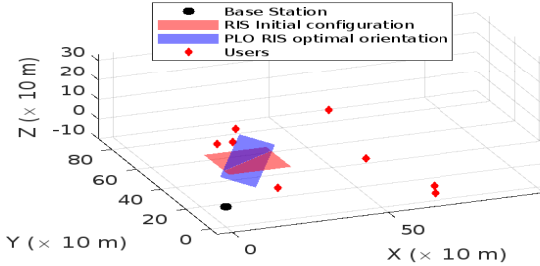


Fig. 3. Optimal RIS orientation for PLO.

$d_{H_0} = \frac{\lambda}{2}$ and $d_{V_0} = \frac{\lambda}{2}$, respectively. The RIS number of elements is $M_H \times M_V = 5 \times 4$, and the horizontal and vertical separation distances of the RIS are $d_{H_R} = \frac{\lambda}{2}$ and $d_{V_R} = \frac{\lambda}{2}$. The o-MRAV coordinates x_R , y_R , and z_R are constrained to $x_R \in [0, 1000m]$, $y_R \in [0, 1000m]$, and $z_R \in [150m, 300m]$, respectively. We suppose the reference gain at 1m is $\beta_0 = -30dB$, the noise power is $\sigma^2 = -100dBm$ [22], and the bandwidth of each user is $B_k = 10MHz$. For the p -norm approximation in problem (15), we consider $p = -8$.

We evaluate the following three approaches: i) PLO: This scheme is the proposed approach described in the section. III, where the RIS phase shift, The MRAV location, and orientation are all optimized by PSCA. ii) PL: This scheme consists in phase shift and location optimization using PSCA. It corresponds to traditional optimization found in the literature for UAV-carried RIS scenarios [23] [24]. iii) PO: This approach consists of phase shift and RIS orientation optimization through PSCA, with a fixed position of MRAV set on top of the barycenter of all users, at the optimal altitude obtained through PLO.

In Fig. 2(a), we plot the minimum data rate against the number of iterations, obtained by averaging over 10 simulations. As can be seen, PLO achieved the best performance, followed by PL, and PO schemes. PLO achieved a minimum data rate of 28%, and 80% high compared to PL and PO, respectively. The reason of PL's under-performance compared to PLO is that in addition to phase shift and location, PLO also optimizes the orientation of the RIS, thanks to the o-MRAV's ability to control both position and orientation independently.

The PO scheme's poor performance is due to its fixed MRAV location, which highlights the importance of optimizing the MRAV location first; orientation optimization further enhances performance when the location is optimal.

Fig. 2(b) plots the average data rate of users against the number of iterations, obtain by averaging over 10 simulations. The same trend as in Fig. 2(a) is observed. PLO performs 14% and 69% higher than PL and PO, respectively. This shows the overall gain achieved in terms of data rate through the joint optimization of MRAV location and RIS orientation. Additionally, by maximizing the minimum data rate among users, the network's average data rate is improved.

Fig. 2(c) illustrates one of the network configurations under consideration, which shows the final positions achieved by the ARIS for all schemes. We observe that the MRAV positions for PLO and PL are near the base station at an altitude close to the minimum of 150 m due to minimal path loss experienced by the received signal in this area. Thanks to the RIS, the signal can then be transmitted through passive beamforming to users over long distances.

In Fig. 3, the final orientation of the PLO RIS, for one of the network configurations under consideration, is plotted. The figure shows the scheme's ability to vary the RIS's orientation while maintaining visibility with both the base station and the users.

V. CONCLUSION

In this paper, we investigate the use of o-MRAV deployed as relays for terrestrial communication in obstructed environments. The emphasis was on the joint optimization of the o-MRAV orientation and position, and the RIS phase shift to maximize the minimum data rate among users. To tackle the challenging studied problem, a close smooth approximation was used and then the problem was solved using PSCA. Through simulation experiments, we showed that o-MRAV independent orientation and location control enhance both the minimum rate and the average rate by 28% and 14%, respectively, compared to traditional u-MRAV. In future works, we are planning to investigate o-MRAV-equipped RIS deployment to combat eavesdropping. We will also investigate the energy efficiency of o-MRAV-equipped RIS when used as relays to assist terrestrial communication.

REFERENCES

- [1] Abdoul Karim A. H. Saliyah, Doha Hamza, Hajar El Hammouti, Jeff S. Shamma, and Mohamed-Slim Alouini, "Multi-sided matching for space-air-ground integrated systems," in *2024 IEEE 99th Vehicular Technology Conference (VTC2024-Spring)*, 2024, pp. 1–7.
- [2] Daniel Bonilla Licea, Mounir Ghogho, and Martin Saska, "When Robotics Meets Wireless Communications: An Introductory Tutorial," *Proceedings of the IEEE*, vol. 112, no. 2, pp. 140–177, 2024.
- [3] Mohammad Mozaffari, Walid Saad, Mehdi Bennis, Young-Han Nam, and Mérouane Debbah, "A Tutorial on UAVs for Wireless Networks: Applications, Challenges, and Open Problems," *IEEE Communications Surveys & Tutorials*, vol. 21, no. 3, pp. 2334–2360, 2019.
- [4] Mouhamed Naby Ndiaye, El Houcine Bergou, Mounir Ghogho, and Hajar El Hammouti, "Age-of-updates optimization for uav-assisted networks," in *GLOBECOM 2022-2022 IEEE Global Communications Conference*. IEEE, 2022, pp. 450–455.
- [5] Mouhamed Naby Ndiaye, El Houcine Bergou, and Hajar El Hammouti, "Multi-agent proximal policy optimization for data freshness in uav-assisted networks," in *2023 IEEE International Conference on Communications Workshops (ICC Workshops)*, 2023, pp. 1920–1925.
- [6] M. Hamandi, F. Usai, Q. Sable, N. Staub, M. Tognon, and A. Franchi, "Design of multirotor aerial vehicles: A taxonomy based on input allocation," *The International Journal of Robotics Research*, vol. 40, no. 8–9, pp. 1015–1044, 2021.
- [7] Daniel Bonilla Licea, Giuseppe Silano, Hajar El Hammouti, Mounir Ghogho, and Martin Saska, "Reshaping uav-enabled communications with omnidirectional multi-rotor aerial vehicles," *IEEE Communications Magazine*, 2025, (to appear).
- [8] Daniel Bonilla Licea, Hajar Elhammouti, Giuseppe Silano, and Martin Saska, "Harnessing the Potential of Omnidirectional Multi-Rotor Aerial Vehicles in Cooperative Jamming Against Eavesdropping," in *IEEE Global Communications Conference*, 2024.
- [9] Daniel Bonilla Licea, Giuseppe Silano, Mounir Ghogho, and Martin Saska, "Omnidirectional Multi-Rotor Aerial Vehicle Pose Optimization: A Novel Approach to Physical Layer Security," in *IEEE International Conference on Acoustics, Speech and Signal Processing*, 2024, pp. 9021–9025.
- [10] H. Lu, Y. Zeng, S. Jin, and R. Zhang, "Aerial intelligent reflecting surface: Joint placement and passive beamforming design with 3D beam flattening," *IEEE Transactions on Wireless Communications*, vol. 20, no. 7, pp. 4128–4143, 2021.
- [11] H.-B. Jeon, S.-H. Park, J. Park, K. Huang, and C.-B. Chae, "An energy-efficient aerial backhaul system with reconfigurable intelligent surface," *IEEE Transactions on Wireless Communications*, vol. 21, no. 8, pp. 6478–6494, 2022.
- [12] Pyae Sone Aung, Yu Min Park, Yan Kyaw Tun, Zhu Han, and Choong Seon Hong, "Energy-efficient communication networks via multiple aerial reconfigurable intelligent surfaces: Drl and optimization approach," *IEEE Transactions on Vehicular Technology*, 2023.
- [13] Y. Cheng, W. Peng, C. Huang, G. C. Alexandropoulos, Chau C. Yuen, and M. Debbah, "RIS-aided wireless communications: Extra degrees of freedom via rotation and location optimization," *IEEE Transactions on Wireless Communications*, vol. 21, no. 8, pp. 6656–6671, 2022.
- [14] S. Zeng, H. Zhang, B. Di, Z. Han, and L. Song, "Reconfigurable intelligent surface (RIS) assisted wireless coverage extension: RIS orientation and location optimization," *IEEE Communications Letters*, vol. 25, no. 1, pp. 269–273, 2020.
- [15] A. Elzanaty, A. Guerra, F. Guidi, and Mohamed-Slim M.-S. Alouini, "Reconfigurable intelligent surfaces for localization: Position and orientation error bounds," *IEEE Transactions on Signal Processing*, vol. 69, pp. 5386–5402, 2021.
- [16] M. Sherman, S. Shao, X. Sun, and J. Zheng, "Optimizing aoi in uav-ris-assisted iot networks: Off policy versus on policy," *IEEE Internet of Things Journal*, vol. 10, no. 14, pp. 12401–12415, 2023.
- [17] E. Björnson, J. Hoydis, and L. Sanguinetti, "Massive mimo networks: Spectral, energy, and hardware efficiency," *Foundations and Trends® in Signal Processing*, vol. 11, no. 3–4, pp. 154–655, 2017.
- [18] B. Zheng, S. Lin, and R. Zhang, "Intelligent reflecting surface-aided leo satellite communication: Cooperative passive beamforming and distributed channel estimation," *IEEE Journal on Selected Areas in Communications*, vol. 40, no. 10, pp. 3057–3070, 2022.
- [19] L. Wei, C. Huang, G. C. Alexandropoulos, C. Yuen, Z. Zhang, and M. Debbah, "Channel estimation for ris-empowered multi-user mimo wireless communications," *IEEE Transactions on Communications*, vol. 69, no. 6, pp. 4144–4157, 2021.
- [20] S. Boyd and L. vandenbergh, "Convex optimization," *Cambridge University Press*, 2004.
- [21] M. Razaviyayn, M. Hong, Z.-Q. Luo, and J.-S. Pang, "Parallel successive convex approximation for nonsmooth nonconvex optimization," in *Advances in Neural Information Processing Systems*, Z. Ghahramani, M. Welling, C. Cortes, N. Lawrence, and K.Q. Weinberger, Eds. 2014, vol. 27, Curran Associates, Inc.
- [22] S. Hu, C. Liu, D. W. K. Ng, and J. Yuan, "Secure communication in multifunctional active intelligent reflection surface-assisted systems," in *WSA and SCC 2023; 26th International ITG Workshop on Smart Antennas and 13th Conference on Systems, Communications, and Coding*, 2023, pp. 1–6.
- [23] H. El Hammouti, A. Saoud, A. Ennahkami, and E.H. Bergou, "Energy efficient aerial ris: Phase shift optimization and trajectory design," in *2024 IEEE Conference on Vehicular Technology (VTC)*. IEEE, 2024.
- [24] Z. Zhai, X. Dai, B. Duo, X. Wang, and X. Yuan, "Energy-efficient uav-mounted ris assisted mobile edge computing," *IEEE Wireless Communications Letters*, vol. 11, no. 12, pp. 2507–2511, 2022.